

Article

N-Heterocyclic Carbene Functionalized Covalent Organic Framework for Transesterification of Glycerol with Dialkyl Carbonates

Yuying Chai ^{1,†}, Yaling Li ^{1,†}, Hui Hu ¹, Chaoyuan Zeng ^{1,*}, Shenglin Wang ¹, Huanjun Xu ^{1,2,*} and Yanan Gao ^{1,*} 

¹ Key Laboratory of Ministry of Education for Advanced Materials in Tropical Island Resources, Hainan University, No 58, Renmin Avenue, Haikou 570228, China; chaiyuying@hainanu.edu.cn (Y.C.); liyaling@hainanu.edu.cn (Y.L.); hhu@hainanu.edu.cn (H.H.); wangshenglin@hainanu.edu.cn (S.W.)

² School of Science, Qiongtai Normal University, No 8, Fuchengzhong Road, Haikou 571127, China

* Correspondence: zengchaoyuan@hainanu.edu.cn (C.Z.); xhj1986@hainanu.edu.cn (H.X.); ygao@hainanu.edu.cn (Y.G.)

† These authors contributed equally to this work.

Abstract: The development of a heterogeneous catalyst through the combination of novel carrier and powerful catalytic active sites is of particular interest. Herein, the successful integration of an N-Heterocyclic carbene (NHC) moiety into a covalent organic framework (COF) was achieved by coupling 4,4',A'',A''''-(pyrene-1,3,6,8-tetrayl) tetraaniline (PyTTA) and equimolar 4,7-bis(4-formylphenyl)-1-methyl-1H-benzimidazole (IM) and 2'3'5'6'-tetrafluoro-[1,1':4',1''-terphenyl]-4,4'-dicarbaldehyde (4F) followed by ionization with 1-bromobutane (C₄H₉Br) and then deprotonation upon addition of a base. The resulting material exhibited promising heterogeneous catalytic activity towards transesterification reaction of glycerol with dialkyl carbonate. Moreover, good recyclability granted no substantial loss of activity upon five cycles. Combination of COFs and NHCs might synergize their characteristics, thus providing more possibilities for creating new patterns of catalytic reactivity.

Keywords: covalent organic framework; carbene; catalyst; glycerol; transesterification



Citation: Chai, Y.; Li, Y.; Hu, H.; Zeng, C.; Wang, S.; Xu, H.; Gao, Y. N-Heterocyclic Carbene

Functionalized Covalent Organic Framework for Transesterification of Glycerol with Dialkyl Carbonates.

Catalysts **2021**, *11*, 423. <https://doi.org/10.3390/catal11040423>

Academic Editor: Antal Csámpai

Received: 15 March 2021

Accepted: 23 March 2021

Published: 26 March 2021

Publisher's Note: MDPI stays neutral with regard to jurisdictional claims in published maps and institutional affiliations.



Copyright: © 2021 by the authors. Licensee MDPI, Basel, Switzerland. This article is an open access article distributed under the terms and conditions of the Creative Commons Attribution (CC BY) license (<https://creativecommons.org/licenses/by/4.0/>).

1. Introduction

Covalent organic frameworks (COFs) are an emerging class of crystalline porous polymer that are composed of organic units linked by reversible covalent bonds or, less commonly, irreversible covalent bonds [1–6]. These materials typically feature large surface areas, well-defined pores, predesignable topological structures, and easy modification, making them intriguing materials for a variety of potential applications pertaining to gas storage/separation [7–13], catalysis [14–26], proton, or ion conduction [27–36], optoelectronics [37–42] and environmental remediation [43–47]. Most COFs for catalysis are constructed through incorporating an existing, powerful, homogeneous catalyst into a linker, which can be achieved through either a “bottom-up” strategy or post-synthetic modification strategy [48,49]. A variety of catalytic active species, including metal ions [15,19,21,50–53] or nanoparticles [54–58], chiral catalyst [23,59], and ionic liquids [60–62] have been successfully introduced into the framework to obtain catalytic COF materials that exhibited excellent catalytic performance in various organic reactions, such as Suzuki–Miyaura coupling [15], Michael addition reaction [63], Heck reaction [64], Henry reaction [65], and some cascade reactions [21,66,67]. Besides, a π -electronic COF was developed as an activator to facilitate Diels–Alder reaction [68].

N-Heterocyclic carbenes (NHCs) are another class of powerful catalysts that would be appealing to feature in COFs. In homogeneous catalysis, they are found to be highly effective for a broad range of rearrangement, addition, and group-transfer reactions entailing carbon–carbon, carbon–nitrogen, and carbon–oxygen bond formation or deletion [69–73].

The immobilization of NHCs not only broadens their application range but also provides new solutions for challenges in catalytic and synthetic chemistry [74], for instance, transforming reactions from homogeneous into heterogeneous catalysis enables effective catalyst/product separation for reuse, especially when separation and waste disposal are high-cost. In a variety of catalysis carriers, silica- (i.e., zeolites) and carbon-based (i.e., graphene, carbon nanotubes) materials are the most frequently used Supporting Materials. Recently, a growing interest in the use of metal–organic frameworks (MOFs) as carriers for NHC immobilization emerges as they enable the uniform distribution of NHC active sites in a controllable way [75–78]. However, MOFs are subjected to degradation upon the addition of bases required to deprotonate heterocyclic carbon atoms or unwanted recruitment of metal ions at the intended carbene sites during the syntheses of MOFs [74].

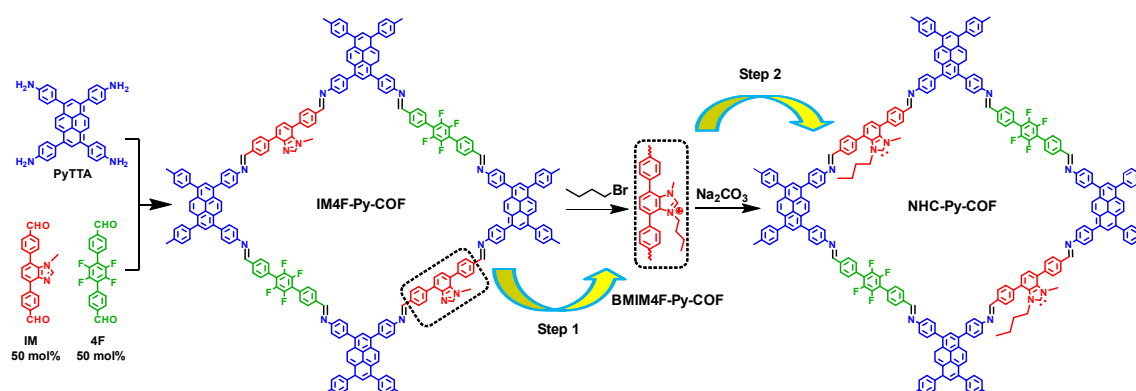
COFs are constructed from organic building units linked by strong covalent bonds, which can essentially avoid the aforementioned problems met by MOFs. As such, the incorporation of NHCs into COF skeletons will provide an intriguing strategy for the development of heterogeneous NHC catalysts, especially considering the unique features of COFs, i.e., large surface area, flexible regulation of pore size, shape, and size distribution, as well as a one-dimensional (1D) open channel structure that facilitates fast diffusion of substances. In addition to the fundamental advantage of heterogeneous catalysts in product separation, we envisage that using COFs as catalytic carriers for the immobilization of NHCs would (1) endow the chemical reactions with shape-, size-, chemo-, or enantio-selectivity owing to well-defined pore environment; (2) allow spatial separation of multiple catalytic sites in a framework that generally cannot co-exist compatibly in homogeneous systems (like NHCs and Lewis acidic metal ions), thereby providing more possibilities for creating new patterns of catalytic reactivity; (3) enhance catalyst reactivity due to cooperative catalysis character of multiple catalytic sites. With this in mind, we report on the post-synthetic modification strategy of a COF for NHC functionalization. Considering that nucleophilic N-heterocyclic carbenes are efficient catalysts for transesterification reactions in homogeneous catalytic systems [79,80], we investigated the transesterification of glycerol with dialkyl carbonates using *in situ* generated NHC-functionalized COF as a heterogeneous catalyst. It was found that the NHC-functionalized COF also presented its effectiveness in transesterification. Note that NHC-based COFs have recently been reported and exhibited outstanding catalytic performance in carboxylation reaction [81] and hydrogenation of reaction [82]. However, noble metals were decorated in these studies. It is the first time that a metal-free NHC-functionalized COF was reported as a catalyst in this work.

2. Results and Discussion

2.1. Synthesis and Characterization of COFs

An imine-linked COF, IM4F-Py-COF, was initially synthesized via a three-component condensation reaction, in which 4,4',4'',4'''-(pyrene-1,3,6,8-tetrayl) tetraaniline (PyTTA) was used as the vertices and two linear dialdehyde monomers, namely 4,7-bis(4-formylphenyl)-1-methyl-1H-benzimidazole (IM) and 2',3',5',6'-tetrafluoro-[1,1':4',1''-terphenyl]-4,4'-dicarbaldehyde (4F), were used as edges (Scheme 1). The molar ratio of IM to 4F was set at 1:1 because fluoro-substituted and non-substituted units at an equimolar ratio would produce the strongest self-complementary interlayer interactions [83]. As a control, 4F-Py-COF was also prepared through the condensation of 4F and PyTTA, i.e., only 4F was used as edges. Post-synthetic modification of IM4F-Py-COF was achieved through the quaternization reaction of benzimidazole groups on the skeleton with 1-bromobutane (C₄H₉Br) to produce ionic BMIM4F-Py-COF, which was then transformed into NHC-functionalized NHC-Py-COF in the presence of NaCO₃. In other words, BMIM4F-Py-COF is a pre-catalyst in this research. Each benzimidazole framework can be essentially treated as a discrete molecule to undergo a reaction normally performed in molecular organic chemistry, providing a completely different framework material. The catalytic performance of the resulting NHC-Py-COF was then evaluated by the transesterification reaction of glycerol with dialkyl

carbonates and excellent catalytic activity and good recyclability were observed for the NHC-Py-COF.



Scheme 1. Synthesis of NHC-Py-COF.

The crystalline nature of all the COFs was confirmed by powder X-ray diffraction (PXRD) measurements. IM4F-Py-COF exhibited strong diffraction peaks at 2.8° , 3.8° , 5.5° , 8.2° , 10.9° , 13.7° , and 23.2° , which were attributed to the (110), (020), (220), (330), (400), (550), and (001) facets, respectively (Figure 1a, red curve). The use of lattice modeling (Figure 1a, magenta curve) and Pawley refinement processes produce an eclipsed AA stacking model that reproduced the PXRD pattern very well with R_{wp} of 2.9% and R_p of 1.6% (Figure 1a, black curve). The Pawley refinement using the unit cell parameters of $a = 49.83 \text{ \AA}$, $b = 42.60 \text{ \AA}$, $c = 3.93 \text{ \AA}$, and $\alpha = \beta = \gamma = 90^\circ$, confirmed the peak assignment, as evidenced by the negligible difference (Figure 1a, blue curve). By contrast, an alternatively staggered AB model did not match the observed data (Figure 1a, olive curve). A schematic arrangement structure was shown in Figure 1b. Moreover, identical PXRD patterns were also observed for BMIM4F-Py-COF and 4F-Py-COF, suggesting that these three COFs possess similar crystal structures (Figure 2). The slight decrease in the diffraction peak intensity of BMIM4F-Py-COF was attributed to the occupation of the pores by the grafted n-butyl groups.

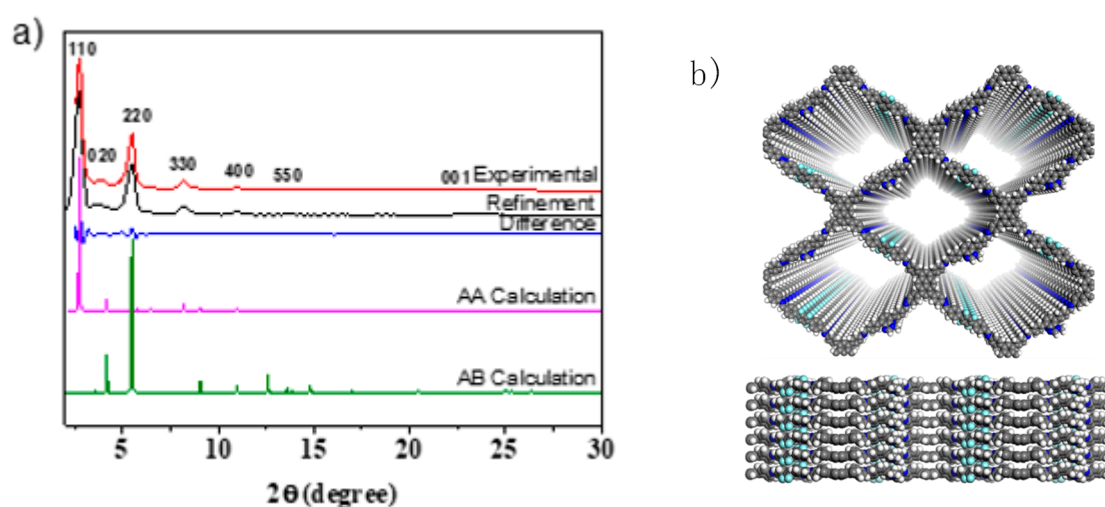


Figure 1. (a) PXRD patterns of IM4F-Py-COF. Observed XRD pattern (red) and profiles simulated using the Pawley refinement (black), their difference (blue), AA-stacking (magenta), and AB-stacking (olive) modes of the IM4F-Py-COF; (b) Schematic arrangement structure of IM4F-Py-COF.

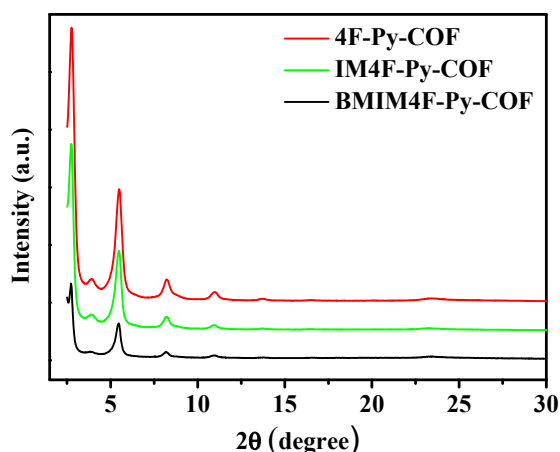


Figure 2. Comparison of PXRD patterns of IM4F-Py-COF (green), BMIM4F-Py-COF (black), and 4F-Py-COF (red).

FT-IR spectroscopy was used to characterize the formation and modification of the COFs. As shown in Figure 3, a strong characteristic stretching peak at 1622 cm^{-1} was observed for all COFs, revealing imine ($-\text{C}=\text{N}-$) linkages of these COFs. Besides, a strong peak appeared at 980 cm^{-1} , which can be ascribed to the $-\text{C}-\text{F}-$ stretching vibration. In IM4F-Py-COF and BMIM4F-Py-COF, the peak at 1072 cm^{-1} was due to the $-\text{C}-\text{N}-$ stretching vibration, which was absent in 4F-Py-COF. A new peak that appeared at 2956 cm^{-1} in BMIM4F-Py-COF was ascribed to the characteristic stretching of $-\text{CH}_2-$, indicating the successful grafting of n-butyl groups onto the channel walls.

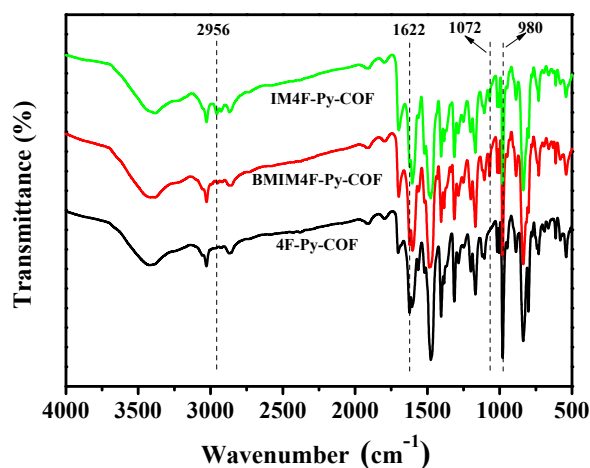


Figure 3. FT-IR spectra of IM4F-Py-COF, BMIM4F-Py-COF, and 4F-Py-COF.

The porous properties of all the COFs were characterized by nitrogen adsorption-desorption isotherms measured at 77 K. As shown in Figure 4a, the three COFs exhibited the typical type-IV adsorption isotherms, indicative of mesoporous characteristics. The BET surface areas were measured to be 1930 , 1450 , and $1326\text{ m}^2\text{ g}^{-1}$, and the pore widths were calculated to be 3.43 , 3.34 , and 3.31 nm for 4F-Py-COF, IM4F-Py-COF, and BMIM4F-Py-COF, respectively (Figure 4b–d). Their corresponding total pore volumes were calculated to be 1.82 , 1.11 , and $0.65\text{ cm}^3\text{ g}^{-1}$, respectively (Table 1). Based on the PXRD and adsorption isotherm results, it is evident that the ordered framework structure remained after modification.

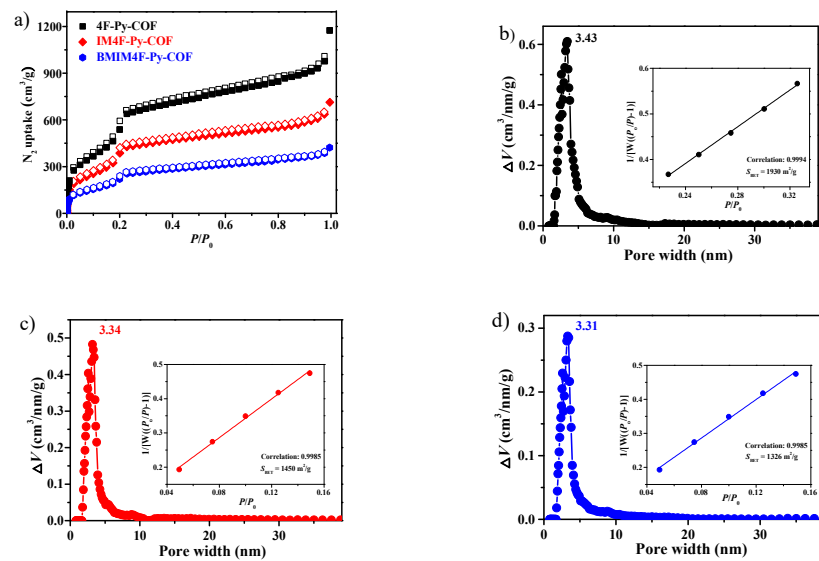


Figure 4. N_2 adsorption-desorption isotherms (a) and their pore size distribution of IM4F-Py-COF (b), BMIM4F-Py-COF (c), and 4F-Py-COF (d) recorded at 77 K, respectively.

Table 1. Porous properties of 4F-Py-COF, IM4F-Py-COF, and BMIM4F-Py-COF.

COFs	S_{BET} ($m^2 g^{-1}$)	Pore Width (nm)	Total Pore Volume ($cm^3 g^{-1}$)
4F-Py-COF	1930	3.43	1.82
IM4F-Py-COF	1450	3.34	1.11
BMIM4F-Py-COF	1326	3.31	0.65

The thermal behavior of the three COFs was detected by thermogravimetric analysis (TGA). It can be seen from Figure 5 that all the materials decomposed at a temperature above 450 °C, indicating their good thermal stability. The decomposition temperature of IM4F-Py-COF is higher than 4F-Py-COF. This result suggests that strong interlayer interaction stemming from a fluoro-substituted and non-substituted unit combination leads to high thermal stability. After the ionization modification, the thermal stability slightly decreased, as reflected by the weight loss at ca. 200 °C, which may be attributed to the decomposition of an ionic moiety attached to the channel walls. However, the frameworks still remain at high thermal stability (>450 °C). Therefore, it is practicable for BMIM4F-Py-COF to be used as a pre-catalyst for the transesterification of glycerol with dialkyl carbonates.

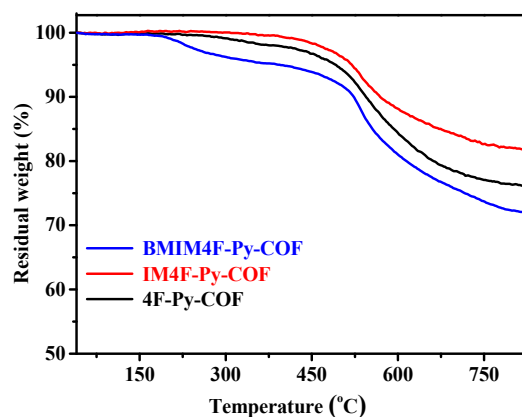


Figure 5. TGA curves of IM4F-Py-COF, BMIM4F-Py-COF, and 4F-Py-COF.

The use of 1-alkylimidazolium type ionic liquid and CO₂ in the presence of a base as a precatalyst for carbene has been widely reported and the formed carbene catalysts exhibited excellent catalytic performance in carboxylation reaction [84], reduction reactions [85], and cycloaddition reaction [86]. Moreover, the NHC-functionalized polymer was also used for reversible fixation-release of CO₂ [87]. During these reactions, an intermediate *N*-heterocyclic carbene (NHC)-CO₂ zwitterionic adduct was formed in situ that was then subjected to nucleophilic substitution reaction to give final products due to its strong σ -donor character. In our case, although benzimidazolium moiety was integrated into the skeleton of COF, we assume that the deprotonation to form NHC in the heterogeneous system could also happen just like in a molecular solution.

2.2. Catalytic Performance of COFs.

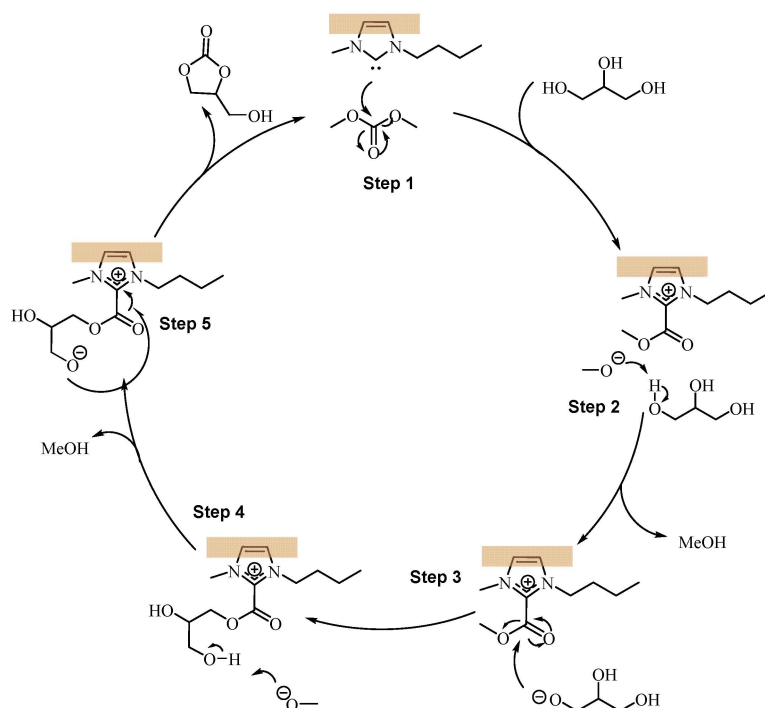
The catalytic activity of the COF was tested in the transesterification reaction of glycerol with dialkyl carbonates by the in situ generated NHC-Py-COF catalyst [88,89]. The reactions were performed at 70 °C, and the reaction time was 8 h. In these reactions, a 5 mol% NHC-Py-COF catalyst, generated through the addition of 2.5 mol% Na₂CO₃ into BMIM4F-Py-COF, was used. The catalytic performance is summarized in Table 2. The transesterification of glycerol with dimethyl carbonate (DMC) was used as a model reaction. The reaction cannot proceed without a catalyst (Table 2, entry 1), which is in accordance with previously reported literature [90,91]. On the contrary, high conversion (99%) and yield (96%) were obtained when NHC-Py-COF was used as a catalyst (Table 2, entry 2). A similar result was also observed for the transesterification reaction of glycerol with diethyl carbonate (96% for both conversion and yield, Table 2, entry 3). Such high catalytic activity is comparable to that of NHC-[BMIM]Br (Table 2, entry 4), suggesting that the heterogeneous NHC-Py-COF catalyst possesses an excellent catalytic ability that can only be achieved by a corresponding homogenous counterpart. In addition, [BMIM]Br, IM4F-Py-COF, and 4F-Py-COF were tried to catalyze the model reaction, no product can be detected, indicating that the reaction was catalyzed by NHC-Py-COF (Table 2, entry 5–7). The separation and recyclability of the catalyst are further investigated for this heterogeneous reaction. After each cycle, the NHC-Py-COF could be simply regenerated by centrifugation. As shown in Table 2, entry 8–12, the catalyst NHC-Py-COF could be reused at least 5 times without significant loss of its catalytic activity.

Table 2. Transesterification of glycerol with dialkyl carbonates over NHC-Py-COF. [a].

Entry	Catalyst	Substrate (R=)	Conversion [b] (%)	Yield [b] (%)
1	Blank	CH ₃	—	—
2	NHC-Py-COF	CH ₃	99	96
3	NHC-Py-COF	CH ₂ CH ₃	96	96
4	NHC-[BMIM]Br	CH ₃	99	99
5	[BMIM]Br	CH ₃	—	—
6	IM4F-Py-COF	CH ₃	—	—
7	4F-Py-COF	CH ₃	—	—
8 [c]	NHC-Py-COF	CH ₃	99	95
9 [d]	NHC-Py-COF	CH ₃	98	95
10 [e]	NHC-Py-COF	CH ₃	98	94
11 [f]	NHC-Py-COF	CH ₃	97	94
12 [g]	NHC-Py-COF	CH ₃	95	93

[a] Reaction condition: catalyst 5 mol%, glycerol (2.5 mmol), dialkyl carbonate (7.5 mmol), 70 °C, 8h. [b] Determined by GC and confirmed by ¹H NMR analysis. [c–g] Cycle from one to five times, respectively.

Based on our experiments and previous literature, we propose the following mechanism for this reaction (Scheme 2). Take DMC as an example, in situ generated carbene on the skeleton of COF attacks the carbon of the carbonyl group of DMC, leading to the cleavage of one methoxy anion (Step 1), that in turn deprotonates the primary alcohol group of glycerol (Step 2). The generated alkoxide then attracts the carbonyl group on the 1-butyl-3-methylimidazole complex. As a result, the other methoxy anion is lost (Step 3). This methoxy anion then deprotonates the secondary alcohol group (Step 4), giving an alkoxide attached to the 1-butyl-3-methylimidazole complex. This alkoxide then attacks the carbonyl carbon of the complex to produce the product and meanwhile regenerates the active carbene species (Step 5).



Scheme 2. Proposed reaction mechanism of the transesterification of glycerol and DMC.

3. Experimental

3.1. Materials

All starting materials and solvents, unless otherwise specified, were obtained from commercial resources and used without further purification. Three building units, 4,4',4'',4'''-(pyrene-1,3,6,8-tetrayl)tetraaniline (PyTTA), 4,7-bis(4-formylphenyl)-1-methyl-1H-benzimidazole (IM), and 2'3'5'6'-tetrafluoro-[1,1':4',1''-terphenyl]-4,4'-dicarbaldehyde (4F) were synthesized according to published procedures [92–94]. All reactions were performed at ambient laboratory conditions, and no precautions were taken to exclude oxygen or atmospheric moisture unless specified.

3.2. Synthesis

Synthesis of IM4F-Py-COF. PyTTA (21.67 mg, 0.04 mmol), IM (13.76 mg, 0.04 mmol), and 4F (14.32 mg, 0.04 mmol) were placed in a glass ampule vessel (10 mL), followed by adding 2 mL of 1,2-dichlorobenzene as a solvent. The mixture was sonicated for 10 min and 0.2 mL of 6.0 M acetic acid was rapidly added. The vessel was then flash-frozen in liquid nitrogen and degassed by three freeze-pump-thaw cycles. The internal pressure of the vessel was controlled below 5 Pa. The system was rapidly sealed with a flame, and then heated at 120 °C for 3 days. The resulting precipitate is filtered out, washed thoroughly with anhydrous THF and acetone to give a yellow colored powder, which was dried at 100 °C under vacuum overnight to give the desired product in 78% yield.

Synthesis of BMIM4F-Py-COF. IM4F-Py-COFT measuring 50 mg, 5 mL of 1-bromobutane, and 20 mL of acetonitrile were added to a 50 mL round-bottom flask. The reaction was heated under reflux at 80 °C and stirred for 48 h. After cooling down to room temperature, the precipitate of the product was collected by filtration, and washed thoroughly with anhydrous ethanol and acetone, respectively. The precipitate was then dried at 100 °C overnight under vacuum, giving a dark yellow product in 95% yield.

Synthesis of 4F-Py-COF. PyTTA (21.67 mg, 0.04 mmol), and 4F (28.64 mg, 0.08 mmol) were placed in a glass ampule vessel (10 mL), followed by adding 2 mL of 1,2-dichlorobenzene. The mixture was sonicated for 10 min and 0.2 mL of 6.0 M acetic acid was rapidly added. The vessel was then flash-frozen in liquid nitrogen and degassed by three freeze-pump-thaw cycles. The internal pressure of the vessel was controlled below 5 Pa. The system was rapidly sealed with a flame, and then heated at 120 °C for 3 days. The resulting precipitate was filtered out and washed thoroughly with anhydrous THF and acetone to give a yellow-colored powder, which was dried at 100 °C under vacuum overnight to give the desired product with 81% yield.

3.3. General Procedures for Transesterification of Glycerol with Dialkyl Carbonates

In a typical experiment, the reaction was performed using a 5 mol% catalyst (generated in situ by a 5 mol% pre-catalyst and 2.5 mol% Na₂CO₃), 2.5 mmol of glycerol, and 7.5 mmol of dimethyl carbonate (or diethyl carbonate) at 70 °C for 8 h. No additional solvents were used in this reaction. All experiments were carried out in a Schlenk tube attached with a reflux condenser under an N₂ atmosphere. Dimethyl carbonate and diethyl carbonate were distilled before use. The products were analyzed by flame ionization gas chromatography (GC-17A, Shimadzu), using a capillary column (TC-FFAP). After the reaction, 1 mmol of 1-propanol was added to the reaction solution as an internal standard.

3.4. Characterization

Fourier transform infrared (FT-IR) spectra were recorded using KBr pellets on a Bruker model TENSOR 27 spectrophotometer. Powder X-ray diffraction (PXRD) measurements were recorded on a PANalytical X'Pert model Pro Multipurpose Diffractometer using Cu K_α radiation at 40 kV and 40 mA. The signals were collected from 2θ of 2.5–30° at a 0.03° step scan with an exposure time of 10 s per step. Low-pressure (0–110 kPa) N₂ gas sorption isotherms were measured volumetrically at 77 K using a Quantachrome Autosorb-iQ2 analyzer with ultrahigh-purity gases. The fresh samples were activated at 100 °C for 15 h under a high vacuum prior to analysis. The Brunauer–Emmett–Teller (BET) model was used to determine the specific surface areas using desorption branches over P/P_0 of 0.01–0.05. In all isotherm plots, closed circles describe adsorption data points and open circles are used to represent desorption data points. The pore size distribution was evaluated by a nonlocal density function theory (NLDFT) method. Thermogravimetric analysis (TGA, STA449F3, NETZSCH, Germany) was performed from room temperature to 800 °C at a heating rate of 10 °C min^{−1} and a N₂ flow rate of 20 mL min^{−1}. Gas chromatography (GC, Agilent 7890A) equipped with a capillary column (HP-5, 30 m × 0.25 mm) using a flame ionization detector. ¹H and ¹³C nuclear magnetic resonance (NMR) spectra were recorded by a Bruker Advance III 400 MHz NMR spectrometer (Bruker BioSpin Corporation, Fällanden, Switzerland).

4. Conclusions

In summary, we developed a post-synthetic modification strategy to anchor N-Heterocyclic carbene (NHC) moiety into a covalent organic framework (COF) that was initially constructed through a three-component condensation reaction. After successful grafting of 1-butyl groups onto the skeletons of the COF, ionization of the framework was achieved, and NHC-functionalized COF, i.e., NHC-Py-COF was then obtained in the presence of a base. The precursors of the NHC-Py-COF were characterized by various technologies. The in situ generated NHC-Py-COF was used as a catalyst for the transesterification reaction of glycerol with dialkyl carbonates. Excellent catalytic activity and good recyclability were

observed, suggesting the excellent catalytic performance of the NHC-functionalized COF. Considering the powerful catalytic activity of NHC and unique features of COFs, we can envisage that the combination of NHC and COF would open up a way to create new patterns of catalytic reactivity.

Supplementary Materials: The following are available online at <https://www.mdpi.com/2073-4344/11/4/423/s1>.

Author Contributions: Conceptualization, C.Z., H.X., Y.G.; Methodology, Y.C., Y.L., S.W.; Formal Analysis, Y.C., Y.L., S.W., C.Z., H.X., H.H., Y.G.; Investigation, Y.C., Y.L., S.W.; Resources, H.X., Y.G.; C.Z. and Y.G. wrote and revised the article. All authors have read and agreed to the published version of the manuscript.

Funding: This work was supported by the Natural Science Foundation of Hainan Province (2019RC166 and 2019RC250) and the National Natural Science Foundation of China (21965011 and 21473196).

Data Availability Statement: Data is contained within the article and Supplementary Material.

Conflicts of Interest: The authors declare no conflict of interest.

References

1. Geng, K.; He, T.; Liu, R.; Tan, K.T.; Li, Z.; Tao, S.; Gong, Y.; Jiang, Q.; Jiang, D.L. Covalent organic frameworks: Design, synthesis, and functions. *Chem. Rev.* **2020**, *120*, 8814–8933. [[CrossRef](#)]
2. Ding, S.Y.; Wang, W. Covalent organic frameworks (COFs): From design to applications. *Chem. Soc. Rev.* **2013**, *42*, 548–568. [[CrossRef](#)]
3. Segura, J.L.; Mancheno, M.J.; Zamora, F. Covalent organic frameworks based on Schiff-base chemistry: Synthesis, properties and potential applications. *Chem. Soc. Rev.* **2016**, *45*, 5635–5671. [[CrossRef](#)]
4. Feng, X.; Ding, X.; Jiang, D.L. Covalent organic frameworks. *Chem. Soc. Rev.* **2012**, *41*, 6010–6022. [[CrossRef](#)] [[PubMed](#)]
5. Chen, X.; Geng, K.; Liu, R.; Tan, K.T.; Gong, Y.; Li, Z.; Tao, S.; Jiang, Q.; Jiang, D.L. Covalent organic frameworks: Chemical approaches to designer structures and built-in function. *Angew. Chem. Int. Ed.* **2020**, *59*, 5050–5091. [[CrossRef](#)] [[PubMed](#)]
6. Hu, H.; Yan, Q.; Ge, R.; Gao, Y. Covalent organic frameworks as heterogeneous catalysts. *Chin. J. Catal.* **2018**, *39*, 1167–1179. [[CrossRef](#)]
7. Du, Y.; Yang, H.; Whiteley, J.M.; Wan, S.; Jin, Y.; Lee, S.H.; Zhang, W. Ionic covalent organic frameworks with spiroborate linkage. *Angew. Chem. Int. Ed.* **2016**, *55*, 1737–1741. [[CrossRef](#)]
8. Zeng, Y.; Zou, R.; Zhao, Y. Covalent organic frameworks for CO₂ capture. *Adv. Mater.* **2016**, *28*, 2855–2873. [[CrossRef](#)] [[PubMed](#)]
9. Baldwin, L.A.; Crowe, J.W.; Pyles, D.A.; McGrier, P.L. Metalation of a mesoporous three-dimensional covalent organic frameworks. *J. Am. Chem. Soc.* **2016**, *138*, 15134–15137. [[CrossRef](#)]
10. Pramudya, Y.; Mendoza-Cortes, J.L. Design principles for high H₂ storage using chelation of abundant transition metals in covalent organic frameworks for 0–700 bar at 298 K. *J. Am. Chem. Soc.* **2016**, *138*, 15204–15213. [[CrossRef](#)]
11. Furukawa, H.; Yaghi, O.M. Storage of hydrogen, methane, and carbon dioxide in highly porous covalent organic frameworks for clean energy applications. *J. Am. Chem. Soc.* **2009**, *131*, 8875–8883. [[CrossRef](#)]
12. Huang, N.; Chen, X.; Krishna, R.; Jiang, D. Two-dimensional covalent organic frameworks for carbon dioxide capture through channel-wall functionalization. *Angew. Chem. Int. Ed.* **2015**, *54*, 2986–2990. [[CrossRef](#)]
13. Huang, N.; Krishna, R.; Jiang, D.L. Tailor-made pore surface engineering in covalent organic frameworks: Systematic functionalization for performance screening. *J. Am. Chem. Soc.* **2015**, *137*, 7079–7082. [[CrossRef](#)]
14. Lin, S.C.; Diercks, S.; Zhang, Y.B.; Kornienko, N.; Nichols, E.M.; Zhao, Y.; Paris, A.R.; Kim, D.; Yang, P.; Yaghi, O.M.; et al. Covalent organic frameworks comprising cobalt porphyrins for catalytic CO₂ reduction in water. *Science* **2015**, *349*, 1208–1213. [[CrossRef](#)] [[PubMed](#)]
15. Ding, S.Y.; Gao, J.; Wang, Q.; Zhang, Y.; Song, W.G.; Su, C.Y.; Wang, W. Construction of covalent organic framework for catalysis: Pd/COF-LZU1 in Suzuki-Miyaura coupling reaction. *J. Am. Chem. Soc.* **2011**, *133*, 19816–19822. [[CrossRef](#)] [[PubMed](#)]
16. Vyas, V.S.; Haase, F.; Stegbauer, L.; Savasci, G.; Podjaski, F.; Ochsenfeld, C.; Lotsch, B.V. A tunable azine covalent organic framework platform for visible light-induced hydrogen generation. *Nat. Commun.* **2015**, *6*, 1–9. [[CrossRef](#)] [[PubMed](#)]
17. Sun, Q.; Aguila, B.; Perman, J.; Nguyen, N.; Ma, S. Flexibility matters: Cooperative active sites in covalent organic framework and threaded ionic polymer. *J. Am. Chem. Soc.* **2016**, *138*, 15790–15796. [[CrossRef](#)]
18. Wang, X.; Han, X.; Zhang, J.; Wu, X.; Liu, Y.; Cui, Y. Homochiral 2D porous covalent organic frameworks for heterogeneous asymmetric catalysis. *J. Am. Chem. Soc.* **2016**, *138*, 12332–12335. [[CrossRef](#)] [[PubMed](#)]
19. Zhang, J.; Han, X.; Wu, X.; Liu, Y.; Cui, Y. Multivariate chiral covalent organic frameworks with controlled crystallinity and stability for asymmetric catalysis. *J. Am. Chem. Soc.* **2017**, *139*, 8277–8285. [[CrossRef](#)]
20. Xu, H.S.; Ding, S.Y.; An, W.K.; Wu, H.; Wang, W. Constructing crystalline covalent organic frameworks from chiral building blocks. *J. Am. Chem. Soc.* **2016**, *138*, 11489–11492. [[CrossRef](#)]

21. Leng, W.; Peng, Y.; Zhang, J.; Lu, H.; Feng, X.; Ge, R.; Dong, B.; Wang, B.; Hu, X.; Gao, Y. Sophisticated design of covalent organic frameworks with controllable bimetallic docking for a cascade reaction. *Chem. Eur. J.* **2016**, *22*, 9087–9091. [[CrossRef](#)]
22. Sun, Q.; Tang, Y.; Aguila, B.; Wang, S.; Xiao, F.S.; Thallapally, P.K.; Al-Enizi, A.M.; Nafady, A.; Ma, S. Reaction environment modification in covalent organic frameworks for catalytic performance enhancement. *Angew. Chem. Int. Ed.* **2019**, *131*, 8762–8767. [[CrossRef](#)]
23. Bhadra, M.; Kandambeth, S.; Sahoo, M.K.; Addicoat, M.; Balaraman, E.; Banerjee, R. A triazine functionalized porous covalent organic framework for photo-organocatalytic E-Z isomerization of olefins. *J. Am. Chem. Soc.* **2019**, *141*, 6152–6156. [[CrossRef](#)] [[PubMed](#)]
24. Lu, M.; Liu, J.; Li, Q.; Zhang, M.; Liu, M.; Wang, J.L.; Yuan, D.Q.; Lan, Y.Q. Rational design of crystalline covalent organic frameworks for efficient CO₂ photoreduction with H₂O. *Angew. Chem. Int. Ed.* **2019**, *131*, 12522–12527. [[CrossRef](#)]
25. Liu, W.; Li, X.; Wang, C.; Pan, H.; Liu, W.; Wang, K.; Zeng, Q.; Wang, R.; Jiang, J. A scalable general synthetic approach toward ultrathin imine-linked two-dimensional covalent organic framework nanosheets for photocatalytic CO₂ reduction. *J. Am. Chem. Soc.* **2019**, *141*, 17431–17440. [[CrossRef](#)]
26. Zhong, W.; Sa, R.; Li, L.; He, Y.; Li, L.; Bi, J.; Zhuang, Z.; Yu, Y.; Zou, Z. A covalent organic framework bearing single Ni sites as a synergistic photocatalyst for selective photoreduction of CO₂ to CO. *J. Am. Chem. Soc.* **2019**, *141*, 7615–7621. [[CrossRef](#)]
27. Ma, H.; Liu, B.; Li, B.; Zhang, L.; Li, Y.G.; Tan, H.Q.; Zang, H.Y.; Zhu, G. Cationic covalent organic frameworks: A simple platform of anionic exchange for porosity tuning and proton conduction. *J. Am. Chem. Soc.* **2016**, *138*, 5897–5903. [[CrossRef](#)]
28. Chandra, S.; Kundu, T.; Kandambeth, S.; BabaRao, R.; Marathe, Y.; Kunjir, S.M.; Banerjee, R. Phosphoric acid loaded Azo (–N=N–) based covalent organic framework for proton conduction. *J. Am. Chem. Soc.* **2014**, *136*, 6570–6573. [[CrossRef](#)] [[PubMed](#)]
29. Sasmal, H.S.; Aiyappa, H.B.; Bhange, S.N.; Karak, S.; Halder, A.; Kurungot, S.; Banerjee, R. Superprotonic conductivity in flexible porous covalent organic framework membranes. *Angew. Chem. Int. Ed.* **2018**, *130*, 11060–11064. [[CrossRef](#)]
30. Peng, Y.; Xu, G.; Hu, Z.; Cheng, Y.; Chi, C.; Yuan, D.; Cheng, H.; Zhao, D. Mechanoassisted synthesis of sulfonated covalent organic frameworks with high intrinsic proton conductivity. *ACS Appl. Mater. Inter.* **2016**, *8*, 18505–18512. [[CrossRef](#)] [[PubMed](#)]
31. Ranjeesh, K.C.; Illathvalappil, R.; Veer, S.D.; Peter, J.; Wakchaure, V.C.; Goudappagouda; Raj, K.V.; Kurungot, S.; Babu, S.S. Imidazole-linked crystalline two-dimensional polymer with ultrahigh proton-conductivity. *J. Am. Chem. Soc.* **2019**, *141*, 14950–14954. [[CrossRef](#)]
32. Xu, H.; Tao, S.; Jiang, D. Proton conduction in crystalline and porous covalent organic frameworks. *Nat. Mater.* **2016**, *15*, 722–726. [[CrossRef](#)]
33. Hu, Y.; Dunlap, N.; Wan, S.; Lu, S.; Huang, S.; Sellinger, I.; Ortiz, M.; Jin, Y.; Lee, S.H.; Zhang, W. Crystalline lithium imidazolite covalent organic frameworks with high Li-Ion conductivity. *J. Am. Chem. Soc.* **2019**, *141*, 7518–7525. [[CrossRef](#)]
34. Zhang, G.; Hong, Y.L.; Nishiyama, Y.; Bai, S.; Kitagawa, S.; Horike, S. Accumulation of glassy poly(ethylene oxide) anchored in a covalent organic framework as a solid-state Li⁺ electrolyte. *J. Am. Chem. Soc.* **2018**, *141*, 1227–1234. [[CrossRef](#)]
35. Guo, Z.; Zhang, Y.; Dong, Y.; Li, J.; Li, S.; Shao, P.; Feng, X.; Wang, B. Fast ion transport pathway provided by polyethylene glycol confined in covalent organic frameworks. *J. Am. Chem. Soc.* **2019**, *141*, 1923–1927. [[CrossRef](#)]
36. Jeong, K.; Park, S.; Jung, G.Y.; Kim, S.H.; Lee, Y.H.; Kwak, S.K.; Lee, S.Y. Solvent-free, single lithium-ion conducting covalent organic frameworks. *J. Am. Chem. Soc.* **2019**, *141*, 5880–5885. [[CrossRef](#)] [[PubMed](#)]
37. Bertrand, G.H.V.; Michaelis, V.K.; Ong, T.C.; Griffin, R.G.; Dincă, M. Thiophene-based covalent organic frameworks. *Proc. Natl. Acad. Sci. USA* **2013**, *110*, 4923–4928. [[CrossRef](#)] [[PubMed](#)]
38. Calik, M.; Auras, F.; Salonen, L.M.; Bader, K.; Grill, I.; Handloser, M.; Medina, D.D.; Dogru, M.; Löbermann, F.; Trauner, D.; et al. Extraction of photogenerated electrons and holes from a covalent organic framework integrated heterojunction. *J. Am. Chem. Soc.* **2014**, *136*, 17802–17807. [[CrossRef](#)] [[PubMed](#)]
39. Liu, X.H.; Guan, C.Z.; Wang, D.; Wan, L.J. Graphene-like single-layered covalent organic frameworks: Synthesis strategies and application prospects. *Adv. Mater.* **2014**, *26*, 6912–6920. [[CrossRef](#)]
40. Feldblyum, J.I.; McCreery, C.H.; Andrews, S.C.; Kurosawa, T.; Santos, E.J.G.; Duong, V.; Fang, L.; Ayzner, A.L.; Bao, Z.N. Few-layer, large-area, 2D covalent organic framework semiconductor thin films. *Chem. Commun.* **2015**, *51*, 13894–13897. [[CrossRef](#)] [[PubMed](#)]
41. Ding, H.; Li, Y.; Hu, H.; Sun, Y.; Wang, J.; Wang, C.; Wang, C.; Zhang, G.; Wang, B.; Xu, W.; et al. A tetrathiafulvalene-based electroactive covalent organic framework. *Chem. Eur. J.* **2014**, *20*, 14614–14618. [[CrossRef](#)]
42. Spitler, E.L.; Dichtel, W.R. Lewis acid-catalysed formation of two-dimensional phthalocyanine covalent organic frameworks. *Nat. Chem.* **2010**, *2*, 672–677. [[CrossRef](#)] [[PubMed](#)]
43. Sun, Q.; Aguila, B.; Perman, J.; Earl, L.; Abney, C.; Cheng, Y.; Wei, H.; Nguyen, N.; Wojtas, L.; Ma, S. Postsynthetically modified covalent organic frameworks for efficient and effective mercury removal. *J. Am. Chem. Soc.* **2017**, *139*, 2786–2793. [[CrossRef](#)]
44. Huang, N.; Zhai, L.; Xu, H.; Jiang, D. Stable covalent organic frameworks for exceptional mercury removal from aqueous solutions. *J. Am. Chem. Soc.* **2017**, *139*, 2428–2434. [[CrossRef](#)]
45. Ding, S.Y.; Dong, M.; Wang, Y.W.; Chen, Y.T.; Wang, H.Z.; Su, C.Y.; Wang, W. Thioether-based fluorescent covalent organic framework for selective detection and facile removal of mercury(II). *J. Am. Chem. Soc.* **2016**, *138*, 3031–3037. [[CrossRef](#)]
46. Mellah, A.; Fernandes, S.P.S.; Rodríguez, R.; Otero, J.; Paz, J.; Cruces, J.; Medina, D.D.; Djamila, H.; Espiña, B.; Salonen, L.M. Adsorption of pharmaceutical pollutants from water using covalent organic frameworks. *Chem. Eur. J.* **2018**, *24*, 10601–10605. [[CrossRef](#)]

47. Sun, Q.; Aguila, B.; Earl, L.D.; Abney, C.W.; Wojtas, L.; Thallapally, P.K.; Ma, S. Covalent organic frameworks as a decorating platform for utilization and affinity enhancement of chelating sites for radionuclide sequestration. *Adv. Mater.* **2018**, *30*, 1705479–1705487. [[CrossRef](#)] [[PubMed](#)]
48. Rogge, S.M.J.; Bavykina, A.; Hajek, J.; Garcia, H.; Olivos-Suarez, A.I.; Sepúlveda-Escribano, A.; Vimont, A.; Clet, G.; Bazin, P.; Kapteijn, F.; et al. Metal-organic and covalent organic frameworks as single-site catalysts. *Chem. Soc. Rev.* **2017**, *46*, 3134–3184. [[CrossRef](#)]
49. Segura, J.L.; Royuela, S.; Ramos, M.M. Post-synthetic modification of covalent organic frameworks. *Chem. Soc. Rev.* **2019**, *48*, 3903–3945. [[CrossRef](#)]
50. Mu, M.; Wang, Y.; Qin, Y.; Yan, X.; Li, Y.; Chen, L. Two-dimensional imine-linked covalent organic frameworks as a platform for selective oxidation of olefins. *ACS Appl. Mater. Inter.* **2017**, *9*, 22856–22863. [[CrossRef](#)]
51. Feng, X.; Ding, X.; Chen, L.; Wu, Y.; Liu, L.; Addicoat, M.; Irle, S.; Dong, Y.; Jiang, D. Two-dimensional artificial light-harvesting antennae with predesigned high-order structure and robust photosensitising activity. *Sci. Rep.* **2016**, *6*, 1–13. [[CrossRef](#)]
52. Hu, H.; Yan, Q.; Wang, M.; Yu, L.; Pan, W.; Wang, B.; Gao, Y. Ionic covalent organic frameworks for highly effective catalysis. *Chin. J. Catal.* **2018**, *39*, 1437–1444. [[CrossRef](#)]
53. Zhang, Y.; Hu, H.; Ju, J.; Yan, Q.; Arumugam, V.; Jing, X.; Cai, H.; Gao, Y. Ionization of a covalent organic framework for catalyzing the cycloaddition reaction between epoxides and carbon dioxide. *Chin. J. Catal.* **2020**, *41*, 485–493. [[CrossRef](#)]
54. Pachfule, P.; Kandambeth, S.; Diaz, D.D.; Banerjee, R. Highly stable covalent organic framework-Au nanoparticles hybrids for enhanced activity for nitrophenol reduction. *Chem. Commun.* **2014**, *50*, 3169–3172. [[CrossRef](#)]
55. Pachfule, P.; Panda, M.K.; Kandambeth, S.; Shivaprasad, S.M.; Díaz, D.D.; Banerjee, R. Multifunctional and robust covalent organic framework-nanoparticle hybrids. *J. Mater. Chem. A* **2014**, *2*, 7944–7952. [[CrossRef](#)]
56. Bhadra, M.; Sasmal, H.S.; Basu, A.; Midya, S.P.; Kandambeth, S.; Pachfule, P.; Balaraman, E.; Banerjee, R. Predesigned metal-anchored building block for in situ generation of Pd nanoparticles in porous covalent organic framework: Application in heterogeneous tandem catalysis. *ACS Appl. Mater. Inter.* **2017**, *9*, 13785–13792. [[CrossRef](#)]
57. Lu, S.; Hu, Y.; Wan, S.; McCaffrey, R.; Jin, Y.; Gu, H.; Zhang, W. Synthesis of ultrafine and highly dispersed metal nanoparticles confined in a thioether-containing covalent organic framework and their catalytic applications. *J. Am. Chem. Soc.* **2017**, *139*, 17082–17088. [[CrossRef](#)] [[PubMed](#)]
58. Ma, H.C.; Zhao, C.C.; Chen, G.J.; Dong, Y.B. Photothermal conversion triggered thermal asymmetric catalysis within metal nanoparticles loaded homochiral covalent organic framework. *Nat. Commun.* **2019**, *10*, 1–9. [[CrossRef](#)]
59. Xu, H.; Gao, J.; Jiang, D. Stable, crystalline, porous, covalent organic frameworks as a platform for chiral organocatalysts. *Nat. Chem.* **2015**, *7*, 905–912. [[CrossRef](#)]
60. Dong, B.; Wang, L.; Zhao, S.; Ge, R.; Song, X.; Wang, Y.; Gao, Y. Immobilization of ionic liquids to covalent organic frameworks for catalyzing the formylation of amines with CO₂ and phenylsilane. *Chem. Commun.* **2016**, *52*, 7082–7085. [[CrossRef](#)]
61. Jansone-Popova, S.; Moineau, A.; Schott, J.A.; Mahurin, S.M.; Popovs, I.; Veith, G.M.; Moyer, B.A. Guanidinium-based ionic covalent organic framework for rapid and selective removal of toxic Cr(VI) oxoanions from water. *Environ. Sci. Technol.* **2018**, *53*, 878–883. [[CrossRef](#)] [[PubMed](#)]
62. Qiu, J.; Zhao, Y.; Li, Z.; Wang, H.; Shi, Y.; Wang, J. Imidazolium-salt-functionalized covalent organic frameworks for highly efficient catalysis of CO₂ conversion. *ChemSusChem* **2019**, *12*, 2421–2427.
63. Xu, H.; Chen, X.; Gao, J.; Lin, J.B.; Addicoat, M.; Irle, S.; Jiang, D.L. Catalytic covalent organic frameworks via pore surface engineering. *Chem. Commun.* **2014**, *50*, 1292–1294. [[CrossRef](#)]
64. Zhang, J.Q.; Peng, Y.S.; Leng, W.G.; Gao, Y.A.; Xu, F.F.; Chai, J.L. Nitrogen ligands in two-dimensional covalent organic frameworks for metal catalysis. *Chin. J. Catal.* **2016**, *37*, 468–475. [[CrossRef](#)]
65. Li, L.H.; Feng, X.L.; Cui, X.H.; Ma, Y.X.; Ding, S.Y.; Wang, W. Salen-based covalent organic framework. *J. Am. Chem. Soc.* **2017**, *139*, 6042–6045. [[CrossRef](#)]
66. Leng, W.G.; Ge, R.L.; Dong, B.; Wang, C.; Gao, Y.A. Bimetallic docked covalent organic frameworks with high catalytic performance towards tandem reactions. *RSC Adv.* **2016**, *6*, 37403–37406. [[CrossRef](#)]
67. Sun, Q.; Aguila, B.; Ma, S. A bifunctional covalent organic framework as an efficient platform for cascade catalysis. *Mater. Chem. Front.* **2017**, *1*, 1310–1316. [[CrossRef](#)]
68. Wu, Y.; Xu, H.; Chen, X.; Gao, J.; Jiang, D.L. A π -electronic covalent organic framework catalyst: π -walls as catalytic beds for Diels-Alder reactions under ambient conditions. *Chem. Commun.* **2015**, *51*, 10096–10098. [[CrossRef](#)]
69. Lalonde, M.B.; Farha, O.K.; Scheidt, K.A.; Hupp, J.T. *N*-heterocyclic carbene-like catalysis by a metal-organic framework material. *ACS Catal.* **2012**, *2*, 1550–1554. [[CrossRef](#)]
70. Enders, D.; Balensiefer, T. Nucleophilic carbenes in asymmetric organocatalysis. *Acc. Chem. Res.* **2004**, *37*, 534–541. [[CrossRef](#)] [[PubMed](#)]
71. Enders, D.; Niemeier, O.; Henseler, A. Organocatalysis by *N*-heterocyclic carbenes. *Chem. Rev.* **2007**, *107*, 5606–5655. [[CrossRef](#)]
72. Phillips, E.M.; Chan, A.; Scheidt, K.A. Discovering new reactions with *N*-heterocyclic carbene catalysis. *Aldrichim. Acta* **2009**, *42*, 55–66.
73. Ezugwu, C.I.; Kabir, N.A.; Yusubov, M.; Verpoort, F. Metal-organic frameworks containing *N*-heterocyclic carbenes and their precursors. *Coordin. Chem. Rev.* **2016**, *307*, 188–210. [[CrossRef](#)]

74. Zhong, R.; Lindhorst, A.C.; Groche, F.J.; Kühn, F.E. Immobilization of *N*-heterocyclic carbene compounds: A synthetic perspective. *Chem. Rev.* **2017**, *117*, 1970–2058. [[CrossRef](#)]
75. Kong, G.Q.; Ou, S.; Zou, C.; Wu, C.D. Assembly and post-modification of a metal-organic nanotube for highly efficient catalysis. *J. Am. Chem. Soc.* **2012**, *134*, 19851–19857. [[CrossRef](#)] [[PubMed](#)]
76. Kong, G.Q.; Xu, X.; Zou, C.; Wu, C.D. Two metal-organic frameworks based on a double azolium derivative: Post-modification and catalytic activity. *Chem. Commun.* **2011**, *47*, 11005–11007. [[CrossRef](#)]
77. Oisaki, K.; Li, Q.; Furukawa, H.; Czaja, A.U.; Yaghi, O.M. A metal-organic framework with covalently bound organometallic complexes. *J. Am. Chem. Soc.* **2010**, *132*, 9262–9264. [[CrossRef](#)]
78. Burgun, A.; Crees, R.S.; Cole, M.L.; Doonan, C.J.; Sumby, C.J. A 3-D diamondoid MOF catalyst based on in situ generated [Cu(L)₂] *N*-heterocyclic carbene (NHC) linkers: Hydroboration of CO₂. *Chem. Commun.* **2014**, *50*, 11760–11763. [[CrossRef](#)]
79. Grasa, G.A.; Kissling, R.M.; Nolan, S.P. *N*-heterocyclic carbenes as versatile nucleophilic catalysts for transesterification/acylation reactions. *Org. Lett.* **2002**, *4*, 3583–3586. [[CrossRef](#)]
80. Nyce, G.W.; Lamboy, J.A.; Connor, E.F.; Waymouth, R.M.; Hedrick, J.L. Expanding the catalytic activity of nucleophilic *N*-heterocyclic carbenes for transesterification reactions. *Org. Lett.* **2002**, *4*, 3587–3590. [[CrossRef](#)]
81. Li, Y.; Dong, Y.; Kan, J.L.; Wu, X.W.; Dong, Y.B. Synthesis and catalytic properties of metal-*N*-heterocyclic-carbene-decorated covalent organic framework. *Org. Lett.* **2020**, *22*, 7363–7368. [[CrossRef](#)] [[PubMed](#)]
82. Yang, J.J.; Wu, Y.Y.; Wu, X.W.; Liu, W.J.; Wang, Y.F.; Wang, J.W. An *N*-heterocyclic carbene-functionalised covalent organic framework with atomically dispersed palladium for coupling reactions under mild conditions. *Green Chem.* **2019**, *21*, 5267–5273. [[CrossRef](#)]
83. Chen, X.; Addicoat, M.; Irle, S.; Nagai, A.; Jiang, D. Control of crystallinity and porosity of covalent organic frameworks by managing interlayer interactions based on self-complementary π -electronic force. *J. Am. Chem. Soc.* **2013**, *135*, 546–549. [[CrossRef](#)]
84. Tommasi, I.; Sorrentino, F. Utilisation of 1,3-dialkylimidazolium-2-carboxylates as CO₂-carriers in the presence of Na⁺ and K⁺: Application in the synthesis of carboxylates, monomethylcarbonate anions and halogen-free ionic liquids. *Tetrahedron Lett.* **2005**, *46*, 2141–2145. [[CrossRef](#)]
85. Gu, L.Q.; Zhang, Y.G. Unexpected CO₂ splitting reactions to form CO with *N*-heterocyclic carbenes as organocatalysts and aromatic aldehydes as oxygen acceptors. *J. Am. Chem. Soc.* **2010**, *132*, 914–915. [[CrossRef](#)]
86. Liu, X.; Cao, C.S.; Li, Y.F.; Guan, P.; Yang, L.G.; Shi, Y.H. Cycloaddition of CO₂ to epoxides catalyzed by *N*-heterocyclic carbene (NHC)–ZnBr₂ System under mild conditions. *Synlett* **2012**, *23*, 1343–1348. [[CrossRef](#)]
87. Zhou, H.; Zhang, W.Z.; Wang, Y.M.; Qu, J.P.; Lu, X.B. *N*-heterocyclic carbene functionalized polymer for reversible fixation-release of CO₂. *Macromolecules* **2009**, *42*, 5419–5421. [[CrossRef](#)]
88. Burstein, C.; Glorius, F. Organocatalyzed conjugate umpolung of α,β -unsaturated aldehydes for the synthesis of γ -butyrolactones. *Angew. Chem. Int. Ed.* **2004**, *43*, 6205–6208. [[CrossRef](#)]
89. Sohn, S.S.; Rosen, E.L.; Bode, J.W. *N*-heterocyclic carbene-catalyzed generation of homoenolates: γ -Butyrolactones by direct annulations of enals and aldehydes. *J. Am. Chem. Soc.* **2004**, *126*, 14370–14371. [[CrossRef](#)]
90. Pan, S.; Zheng, L.; Nie, R.; Xia, S.; Chen, P.; Hou, Z. Transesterification of glycerol with dimethyl carbonate to glycerol carbonate over Na-based zeolites. *Chin. J. Catal.* **2012**, *33*, 1772–1777. [[CrossRef](#)]
91. Takagaki, A.; Iwatani, K.; Nishimura, S.; Ebitani, K. Synthesis of glycerol carbonate from glycerol and dialkyl carbonates using hydrotalcite as a reusable heterogeneous base catalyst. *Green Chem.* **2010**, *12*, 578–581. [[CrossRef](#)]
92. Huang, N.; Wang, P.M.; Addicoat, A.; Heine, T.; Jiang, D.L. Ionic covalent organic frameworks: Design of a charged interface aligned on 1D channel walls and its unusual electrostatic functions. *Angew. Chem. Int. Ed.* **2017**, *56*, 4982–4986. [[CrossRef](#)]
93. Rabbani, M.G.; Sekizkardes, A.K.; Kahveci, Z.; Reich, T.E.; Ding, R.; El-Kaderi, H.M. A 2D mesoporous imine-linked covalent organic framework for high pressure gas storage applications. *Chem. Eur. J.* **2013**, *19*, 3324–3328. [[CrossRef](#)] [[PubMed](#)]
94. Kuhnert, N.; Patel, C.; Jami, F. Synthesis of chiral nonracemic polyimine macrocycles from cyclocondensation reactions of biaryl and terphenyl aromatic dicarboxaldehydes and 1R,2R-diaminocyclohexane. *Tetrahedron Lett.* **2005**, *46*, 7575–7579. [[CrossRef](#)]